Bol. Soc. Paran. Mat.
©SPM – E-ISSN-2175-1188
SPM: www.spm.uem.br/bspm

(3s.) **v. 2026 (44)** : 1–15.
ISSN-0037-8712
doi:10.5269/bspm.79517

Thermal and Flow Behavior of Paraffin-Based MoS_2, Ag and Cu Nanofluids in Rotating Magnetohydrodynamic (MHD) Systems

Sakeena Bibi, Mukhtar Ahmad, Muhammad Muawwaz*, Fouzia Sadaf and Ather Qayyum

ABSTRACT: This study investigates the thermal performance of silver (Ag), copper (Cu), and molybdenum disulfide (MoS_2) nanoparticles dispersed in paraffin (Pfin) as the base fluid, forming a hybrid nanofluid subjected to three-dimensional rotating flow. The analysis incorporates slip and convective boundary conditions to capture realistic flow behavior. The hybrid nanofluid system Ag-MoS_2-Cu/Pfin is examined with particular emphasis on its influence on heat and mass transport characteristics. An order-reduction numerical algorithm is employed to obtain approximate solutions of the governing flow equations. The effects of key physical parameters are analyzed through graphical and tabular representations of velocity, temperature, and concentration profiles, along with corresponding variations in skin friction, Nusselt number, and Sherwood number. The results reveal that the incorporation of Ag-MoS_2-Cu nanoparticles into paraffin significantly enhances heat transfer rates. Moreover, rotational effects play a critical role in modifying the thermal boundary layer, where increasing rotation intensifies boundary layer thickness. A comparative assessment shows that MoS_2 nanoparticles exhibit superior heat transfer performance relative to Ag and Cu, highlighting their effectiveness in thermal management applications.

Keywords: Molybdenum oxide, silver, paraffin, copper, slip flow, convective conditions, order reduction method.

Contents

1. Introduction

Fluid flows involving rotation and heat transfer play a central role in a wide range of scientific, industrial, and environmental processes. Rotational and electromagnetic effects are fundamental in solar and cosmic physics, while in chemical engineering, rotating flows promote efficient mixing and uniform reactions in industrial reactors. In environmental engineering, rotational currents assist in the dispersion and dilution of pollutants in large water bodies. Similarly, in modern energy systems, rotation-driven mechanisms are essential for energy conversion in hydroelectric turbines and wind turbines, where the kinetic energy of rotating fluids is converted into electrical power. The optimization of rotating flow systems is therefore critical for improving thermal efficiency, energy conversion, and system reliability. Owing to these broad applications, the analysis of rotating flows remains an active and important area of research in fluid mechanics and thermal sciences.

Extensive investigations have been conducted on rotating flow configurations and their influence on heat and momentum transport. Du et al. [1] reported enhanced heat transfer characteristics for a rotating rectangular disk fitted with disjoint fins, where moderate rotation numbers (0–1) produced higher Nusselt numbers. Reddy et al. [2] studied Casson fluid flow over a rotating stretching surface and obtained numerical solutions using MATLAB's `bvp5c` solver. Srilatha et al. [3] analyzed Newtonian fluid flow using a disk–cone configuration, comparing the thermal and flow fields for rotating and stationary cases.

* Corresponding author.
2020 *Mathematics Subject Classification:* 05C90, 05C07.
Submitted October 13, 2025. Published March 28, 2026

The combined influence of disk rotation and surface stretching on thermal and momentum boundary layers was examined in [4]. Shahzad et al. [5] investigated Fe_3O_4 nanofluid flow between two rotating surfaces, one of which was porous, and demonstrated the significant role of Coriolis and centripetal forces. Further studies involving different geometries, base fluids, and nanoparticles under rotational effects can be found in [6,7,8,9,10,33].

Nanofluids have attracted considerable attention due to their superior thermal performance compared with conventional fluids. Berrehal and Maougal [11] analyzed the thermophysical behavior of nanofluids under slip and convective boundary conditions using the optimal homotopy asymptotic method (OHAM). Hybrid nanofluids containing multiple nanoparticles were examined by Rejvani et al. [12], who focused on the rheological characteristics of MWCNTs–SiO_2 mixtures. Qureshi et al. [13] investigated CNT/polymer composites flowing through orthogonal porous disks and showed that increasing the nanolayer thickness in the range 0.4–1.6 significantly enhanced the effective nanolayer thermal conductivity. Buffa et al. [14] studied nanoparticle-based electrodes, while Hadi Seyedi et al. [15] analyzed heat transfer in SWCNTs–H_2O and MWCNTs–H_2O nanofluids in a rotating and expanding channel. Additional contributions to nanofluid modeling and heat transfer analysis can be found in [16,17,18,19,20].

Recent research has emphasized oxide-based nanofluids due to their favorable thermal and chemical properties. Alktranee et al. [21] demonstrated that ZrO_2 nanofluids significantly improve the cooling efficiency of photovoltaic (PV) systems. Souayeh [22] proposed a tri-hybrid nanofluid model to evaluate thermal behavior under rotating conditions. Biomedical and dental applications of nanofluids were reviewed by Cheng et al. [23], while Sun et al. [24] employed neural networks to enhance the prediction of thermophysical properties of oxide nanofluids. Experimental and numerical investigations on turbulent forced convection in oxide-based nanofluids were reported by Guzei et al. [25], further confirming their enhanced thermal performance.

Despite these extensive studies, the thermophysical behavior of hybrid nanofluids containing metallic and layered nanoparticles such as silver (Ag), copper (Cu), and molybdenum disulfide (MoS_2) dispersed in paraffin under three-dimensional rotating flow conditions has not been adequately explored. In particular, the combined effects of slip velocity and convective boundary conditions on heat and mass transfer for such hybrid nanofluids remain largely unexplored. The present work aims to fill this gap by investigating the flow and thermal characteristics of Ag–MoS_2–Cu/paraffin hybrid nanofluids in a rotating system, providing new quantitative insights into their heat and mass transfer enhancement mechanisms.

Paraffin is a class of hydrocarbon compounds primarily composed of long-chain alkanes containing only carbon and hydrogen atoms. In solid form, paraffin wax appears white or colorless, while in its molten state it becomes a transparent liquid. Due to its low melting point, chemical stability, and hydrophobic nature, paraffin is widely used in thermal energy storage, coatings, and industrial applications, making it a suitable base fluid for hybrid nanofluid formulations.

In recent years, researchers have investigated the potential of paraffin as a base fluid for nanofluids by dispersing high-performance nanoparticles such as molybdenum disulfide (MoS_2), copper (Cu), and silver (Ag). These nanoparticles significantly enhance the thermophysical properties of the fluid, making it more effective for heat transfer applications. The novelty of the present study lies in incorporating slip effects and convective boundary conditions into the rotating flow analysis of such nanofluids. Furthermore, this work provides a comparative assessment of the thermal performance of MoS_2/Pfin, Cu/Pfin, and Ag/Pfin systems, highlighting the superior heat transfer capability of MoS_2 in relation to silver and copper.

2. Formulation of the Problem

In the present study, three types of nanoparticles, namely molybdenum disulfide (MoS_2), copper (Cu), and silver (Ag), are considered for the preparation of paraffin (Pfin)-based nanofluids. These nanoparticles are uniformly dispersed into the base fluid to enhance its thermophysical characteristics.

Let Ω denote the angular velocity of the rotating flow over an extended surface. The sheet is aligned with the xy-plane, while the z-axis is taken perpendicular to the surface. Consequently, the angular velocity vector is expressed as $(0, 0, \Omega)$. The velocity components parallel to the surface, u and v, approach their free-stream values far away from the sheet, whereas at the sheet surface they are subjected to slip boundary conditions. The normal velocity component, w, is similarly constrained by the no-penetration

condition at the surface. The schematic structure of the rotating flow configuration is illustrated in Figure 1.

In the current analysis, viscous dissipation and Joule heating are neglected for simplicity. Furthermore, due to the small magnitude of the magnetic Reynolds number, magnetic induction effects are assumed negligible and are not included in the governing equations.

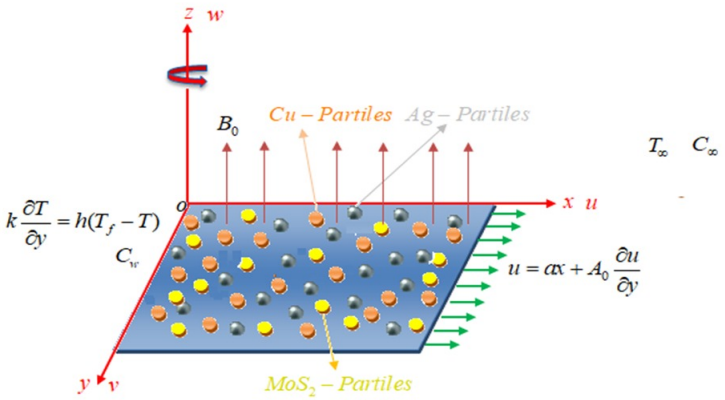

Figure 1: Flow configuration

The above assumptions yield the following governing system of equations [26]:

Equation of continuity:

$$\frac{\partial u}{\partial x}+\frac{\partial v}{\partial y}+\frac{\partial w}{\partial z}=0, \tag{2.1}$$

Momentum equation in the x-direction:

$$\rho_{nf}\left(u\frac{\partial u}{\partial x}+v\frac{\partial u}{\partial y}+w\frac{\partial u}{\partial z}-2\Omega v\right)=\mu_{nf}\frac{\partial^2 u}{\partial z^2}-\sigma B_0^2 u-K, \tag{2.2}$$

Momentum equation in the y-direction:

$$\rho_{nf}\left(u\frac{\partial v}{\partial x}+v\frac{\partial v}{\partial y}+w\frac{\partial v}{\partial z}+2\Omega u\right)=\mu_{nf}\frac{\partial^2 v}{\partial z^2}-\sigma B_0^2 v-K, \tag{2.3}$$

Energy equation:

$$u\frac{\partial T}{\partial x}+v\frac{\partial T}{\partial y}+w\frac{\partial T}{\partial z}=\alpha_{nf}\frac{\partial^2 T}{\partial z^2}+\tau\left[D_B\frac{\partial C}{\partial z}\frac{\partial T}{\partial z}+\frac{D_T}{T_\infty}\left(\frac{\partial T}{\partial z}\right)^2\right], \tag{2.4}$$

Concentration equation:

$$u\frac{\partial C}{\partial x}+v\frac{\partial C}{\partial y}+w\frac{\partial C}{\partial z}=D_B\frac{\partial^2 C}{\partial z^2}+\frac{D_T}{T_\infty}\frac{\partial^2 T}{\partial z^2}. \tag{2.5}$$

The physical meanings of the parameters appearing in the governing equations are summarized in Table 1 (Nomenclature).

The boundary conditions associated with this problem can be expressed as:

$$\begin{aligned} &u=U_s, \quad v=V_s, \quad w=0, \quad T=T_w, \quad C=C_w, \quad \text{at } z=0,\\ &u\to 0, \quad v\to 0, \quad T\to T_\infty, \quad C\to C_\infty, \quad \text{as } z\to\infty, \end{aligned} \tag{2.6}$$

where U_s and V_s denote the slip velocities at the surface, while T_w and C_w represent the wall temperature and concentration, respectively.

By dispersing MoS_2, Cu, and Ag nanoparticles into the base liquid paraffin, three distinct nanofluids are formulated: MoS_2–Pfin, Cu–Pfin, and Ag–Pfin. To accurately evaluate the thermophysical behavior of these nanofluids, the following relations for effective density, heat capacity, viscosity, and thermal conductivity are employed [27]. The effective thermophysical properties of the nanofluids are defined as follows [27]:

Effective density:

$$\rho_{nf} = (1-\phi)\rho_f + \phi\rho_s, \tag{2.7}$$

Heat capacitance:

$$(\rho c_p)_{nf} = (1-\phi)(\rho c_p)_f + \phi(\rho c_p)_s, \tag{2.8}$$

Viscosity:

$$\mu_{nf} = \frac{\mu_f}{(1-\phi)^{2.5}}, \tag{2.9}$$

Thermal conductivity:

$$k_{nf} = k_f \frac{k_s + 2k_f - 2\phi(k_f - k_s)}{k_s + 2k_f + \phi(k_f - k_s)}, \tag{2.10}$$

Nanoparticle volume fraction:

$$\phi = \frac{V_s}{V_s + V_f}, \tag{2.11}$$

where ϕ denotes the nanoparticle volume fraction, ρ the density, c_p the specific heat capacity, μ the dynamic viscosity, and k the thermal conductivity. The subscripts nf, f, and s represent nanofluid, base fluid, and solid nanoparticles, respectively.

Table 2 summarizes the thermophysical properties of molybdenum disulfide (MoS_2), silver (Ag), copper (Cu), and paraffin (Pfin).

Table 1: Thermophysical properties of Ag, Cu, MoS_2, and Paraffin (Pfin) [27].

Property	**Ag**	**Pfin**	**Cu**	**MoS_2**
Specific heat c_p (J/kg·K)	235	2320	385	397.21
Density ρ (kg/m^3)	10500	802	8933	5.06×10^3
Thermal conductivity k (W/m·K)	429	0.23	400	904.4

The variables mentioned below have been incorporated to transform the PDEs (1)–(5) into ODEs:

$$\eta = \sqrt{\frac{a}{v_f}}Z, u = axF^{'}(\eta), v = axg(\eta), w = -\sqrt{av_f}F(\eta) T = T_\infty + (T_w - T_\infty)\theta(\eta), C = C_\infty + (C_w - C_\infty)\theta(\eta) \tag{2.12}$$

The renewed form of the governing equations after applying transformation (2.12) is:

$$F''' + (1-\phi)^{2.5}1 - \phi + \phi\frac{\rho_{nf}}{\rho_f}(FF'' - F'^2 + 2\lambda_0 G) - (1-\phi)^{2.5}M_{00}F' = 0 \tag{2.13}$$

$$G'' + (1-\phi)^{2.5}1 - \phi + \phi\frac{\rho_{nf}}{\rho_f}(FG' - F'G + 2\lambda_0 F') - (1-\phi)^{2.5}M_{00}G = 0 \tag{2.14}$$

$$\theta'' + \frac{Pr}{d_0}F\theta' + \frac{Pr}{d_0}N_b\theta'\phi' + N_t\theta'^2 = 0 \tag{2.15}$$

$$\theta'' + \frac{N_t}{N_b}F\theta'' + Sc_0F\theta' - C_R\theta = 0 \tag{2.16}$$

The transformed boundary conditions are:

$$F'(0) = 1 + S_{lip}F''(0), G(0) = 0, G(0) = 0, \theta(0) = -B_{iot}[1-\theta(0)], \phi(0) = 1, at\eta = 0$$

$$f \to 0, g \to 0, \theta \to 0, \phi \to 0, et.\eta = 0. \tag{2.17}$$

The parameters of the present problem include the magnetic parameter $M = \sigma B_0^2$-Maganetic parameter, and $\Omega = \frac{\omega}{a}$-rotation parameter $B_{iot} = h\sqrt{\frac{v}{a}}/k$-Biot number, and $S_\lambda = A_0\sqrt{\frac{a}{v}}/x$-slip parameter. Furthermore, the Schmidt number $Sc = \frac{v_f}{D_b}$-Schmidt number,and ϕ_1-volume fraction of MoS_2, $Pr = \mu_f(\rho C_p)/\rho k_f$-Prandtl number , and $N_t = \frac{\tau D_T(T_w - T_\infty)}{vT_\infty}$-thermophoresis parameter are incorporated.

Main steps of the numerical procedure:
Step-i: The conversion of PDEs into ODEs using the dimensionless.
Step-ii: Assemble the dimensionless system of equations.
Step-iii: Utilization of Order reduction.
Step-iv: Consolidating of finite differences and Order reduction.
Step-v: Domain meshing and preliminary guesses.
Step-vi: The Proposed boundary condition are satisfied.
Step-vii: Approximate results using numerical simulation.

3. Numerical Approach

The governing system (13)-(16) consists of nonlinear equations, which complicates the derivation of exact analytical solutions. To overcome these difficulties, we adopt a simplified strategy for obtaining approximate solutions. The nonlinear nature of the dimensionless equations restricts direct analytical treatment; therefore, a reduction technique is employed. Specifically, the order of equations (13)-(16) is decreased step by step through suitable substitutions. An iterative numerical scheme with a prescribed convergence tolerance is then applied to compute the approximate solutions. The effectiveness of this scheme has been discussed in detail in [28-31]. The procedure is outlined above, while Table 3 presents a numerical comparison that confirms the accuracy and reliability of the implemented algorithm.

Table 2: Numerical data comparison with Acharya et al. [32].

	$f^{"}(0)$	
λ	Acharya et al. [32]	Present results
0.0	-1.000000	-1.000000
0.5	-1.138381	-1.138350
1.0	-1.325034	-1.325017
2.0	-1.652355	-1.652241

4. Results and Discussion

This section presents the behavior of paraffin-based nanofluids containing Ag, Cu, and MoS_2 nanoparticles. The analysis focuses on the variations of concentration, temperature, and velocity components with respect to the governing parameters.Notable enhancements in the physical characteristics of the nanofluids are observed under different conditions.Throughout the study, the nanoparticle volume fractions of Ag, Cu, and MoS_2 are assumed to remain constant, as is the thermal Prandtl number of the nanofluid. The parameter values employed in the numerical simulations are summarized below. Figures 2-4 illustrate the velocity components and temperature distributions under the influence of the magnetic interaction parameter M.

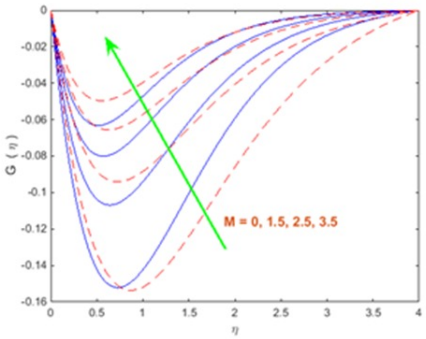

Figure 2: Profile $G(\eta)$ with the parameter

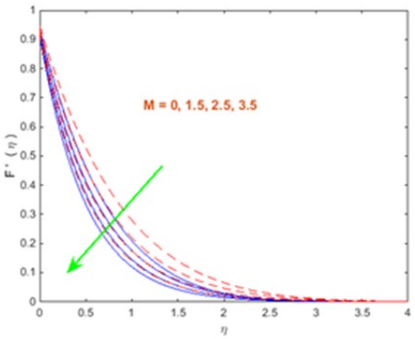

Figure 3: Profile $F^{'}(\eta)$ with the parameter

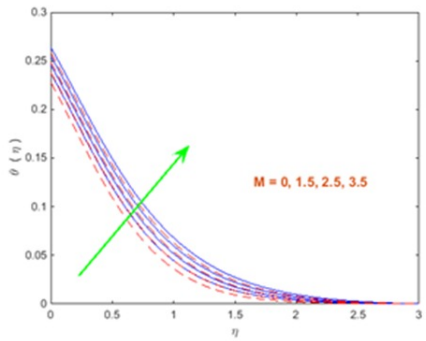

Figure 4: Profile $\theta(\eta)$ with the parameter .

An increase in the magnetic field strength results in a decrease in the x-component of velocity, whereas the y-component exhibits a corresponding increase. For all considered nanofluids (Ag/Pfin, Cu/Pfin, and MoS_2/Pfin), the temperature profile shows a consistent rise with increasing M, confirming the magnetic field's role in enhancing thermal transport. The influence of the rotational parameter on the thermal field is illustrated in Fig. 5, where the temperature distribution increases with rising values of this parameter. Figures 6 and 7 further demonstrate its effect on the velocity components of silver and molybdenum oxide nanofluids. It is observed that as the rotational parameter increases, both velocity components decrease. This behavior can be attributed to the fact that higher stretching rates suppress the rotational effects, thereby reducing fluid motion. Moreover, a comparative assessment reveals that silver (Ag) nanoparticles attain relatively lower temperatures than molybdenum oxide (MoS_2) and copper (Cu) nanoparticles, the latter exhibiting more pronounced thermal enhancement.

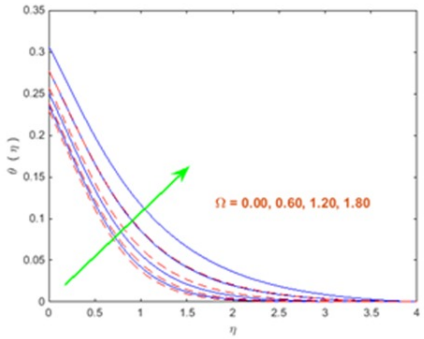

Figure 5: Profile $\theta(\eta)$ with the parameter Ω

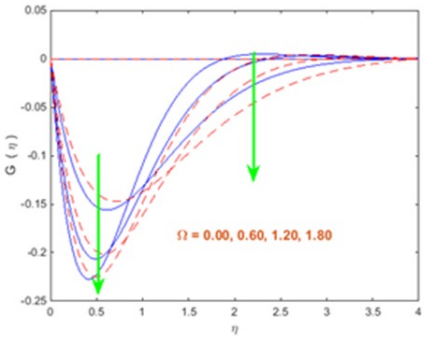

Figure 6: Profile $G(\eta)$ with the parameter Ω

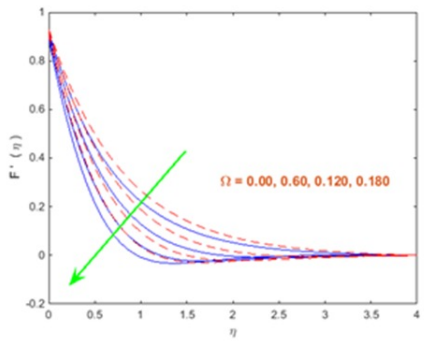

Figure 7: Profile $F^{'}(\eta)$ with the parameter Ω

The influence of the slip parameter on the velocity components is depicted in Figs. 8 and 9. The profiles clearly indicate that the slip parameter plays a significant role: increasing its value reduces both velocity components for all three nanofluid cases, namely Ag/Pfin, Cu/Pfin, and MoS_2/Pfin. The corresponding variations in primary and secondary skin frictions with respect to the slip parameter, magnetic parameter, and rotational parameter are reported in Table 4. It is observed that the slip parameter decreases both primary and secondary skin frictions. In contrast, the magnetic field enhances the primary skin friction while diminishing the secondary skin friction. Similarly, the rotational parameter leads to an increase in both skin friction components.

Table 3: Primary and secondary skin frictions with respect to different parameters.

Parameters			C_{fr_x}			C_{fr_y}		
S_λ	M	Ω	Ag/Pfin	MoS_2/Pfin	Cu/Pfin	Ag/Pfin	MoS_2/Pfin	Cu/Pfin
1.0			-0.72402351	-0.68426644	-0.88412352	0.33978199	0.21500530	0.43938299
2.0			-0.45544885	-0.43878026	-0.55543515	0.24183580	0.15484449	0.37183580
3.0			-0.33439315	-0.32506807	-0.44543231	0.18970223	0.12226161	0.28470121
4.0			-0.26480180	-0.25879919	-0.36883181	0.15667652	0.10141692	0.19665651
	0.0		-0.90599354	-0.81648951	-0.97521312	0.49045775	0.32557133	0.69045672
	1.5		-1.03122105	-0.98541884	-1.73122115	0.32812100	0.19514567	0.57441210
	2.5		-1.09920039	-1.06744763	-1.49922131	0.26671534	0.15335311	0.46671534
	3.5		-1.15584561	-1.13253282	-1.25524521	0.22458055	0.12657867	0.32358152
		0.00	-0.95891275	-0.89149934	-0.98891271	0.41143374	0.25808584	0.35808584
		0.60	-0.97801270	-0.91069035	-0.71801274	0.42254447	0.26717493	0.27432749
		1.20	-0.99010167	-0.93258822	-0.99010163	0.43980142	0.27905810	0.25678493
		1.80	-1.15782364	-0.96253424	-1.05782368	0.44185810	0.28600104	0.38634634

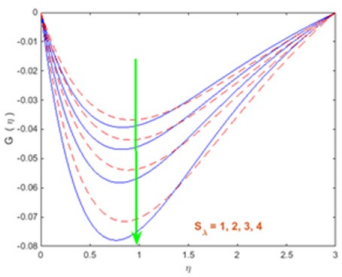

Figure 8: Profile $G(\eta)$ with the parameter S_λ

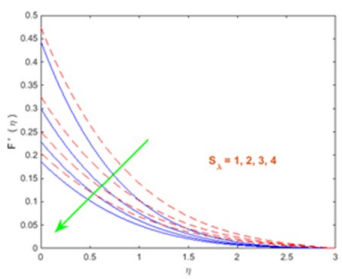

Figure 9: Profile $F^{'}(\eta)$ with the parameter S_λ

The temperature distributions corresponding to different parameters are presented in Figs. 10-13 for Ag/Pfin, Cu/Pfin, and MoS_2/Pfin nanofluids. It is observed that the temperature decreases with an increase in the Prandtl number (Pr) for all three nanofluids. In contrast, the Biot number (Bi), together with the concentration parameters ϕ_1, ϕ_2, and ϕ_3, enhances the thermal profiles, leading to higher temperatures in each case.

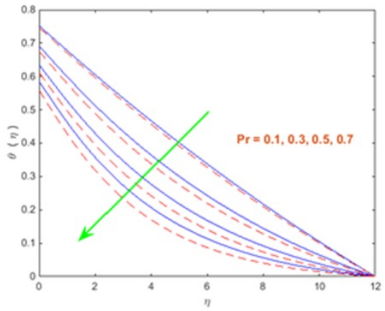

Figure 10: Profile $\theta(\eta)$ with the parameter Pr

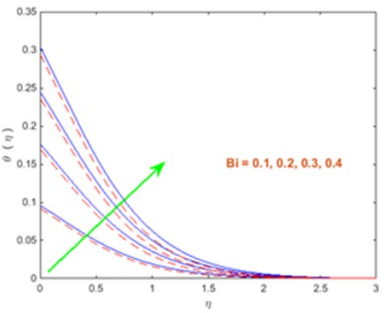

Figure 11: Profile $\theta(\eta)$ with the parameter Bi

The Biot number (Bi) is a dimensionless parameter widely employed in thermal engineering and heat transfer to evaluate the relative significance of convective heat transfer at a solid surface compared to conductive heat transfer within the solid. It is particularly useful in situations where both conduction and convection mechanisms are present, such as heating or cooling of solid bodies in contact with a fluid. Furthermore, the Nusselt number (Nu) is observed to be an increasing function of the Prandtl number (Pr), Biot number (Bi), and the nanoparticle volume fractions ϕ_1, ϕ_2, and ϕ_3, as summarized in Table 5.

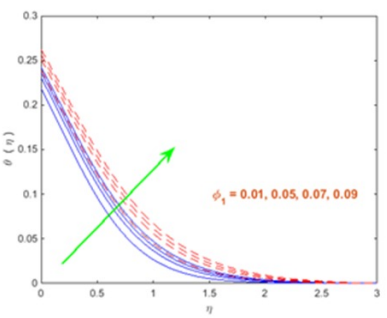

Figure 12: Profile $\theta(\eta)$ with the parameter ϕ_1

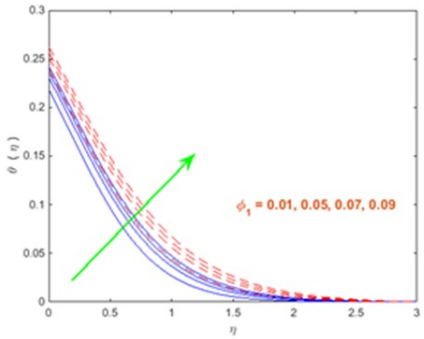

Figure 13: Profile $\theta(\eta)$ with the parameter ϕ_1

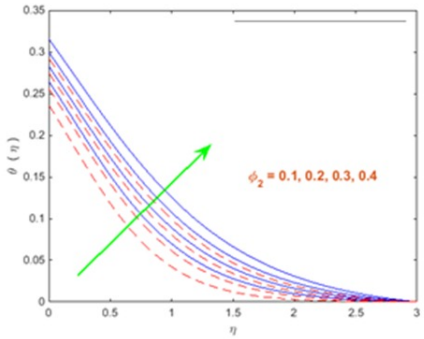

Figure 14: Profile $\theta(\eta)$ with the parameter ϕ_2

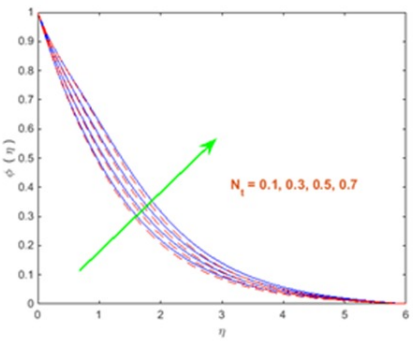

Figure 15: Profile $\phi(\eta)$ with the parameter N_t

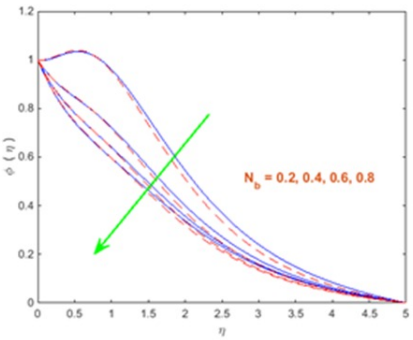

Figure 16: Profile $\phi(\eta)$ with the parameter N_b

Figs. 14-16 illustrate the concentration profiles with respect to the governing parameters. It is evident from these figures that the thermophoretic parameter enhances the temperature field, while the remaining parameters (Brownian motion parameter, Schmidt number, and chemical reaction parameter) exert an opposite influence on the concentration profiles for all nanofluids considered. The thermophoretic parameter, denoted by N_t, is a dimensionless number that quantifies the relative significance of thermophoresis compared to other transport mechanisms in a fluid subjected to temperature gradients, such as convection and diffusion. This parameter plays a key role in fluid dynamics and related disciplines, as its magnitude may alter fluid behavior in diverse ways. The numerical findings presented in Table 6 reveal that increasing N_t markedly decreases the Sherwood number. In contrast, the Brownian motion parameter, Schmidt number, and chemical reaction parameter are observed to enhance the mass transfer rate.

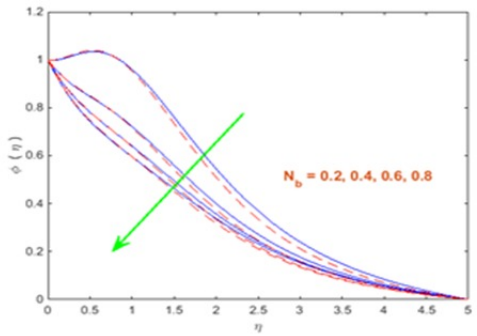

Figure 17: Profile $\phi(\eta)$ with the parameter γ_0

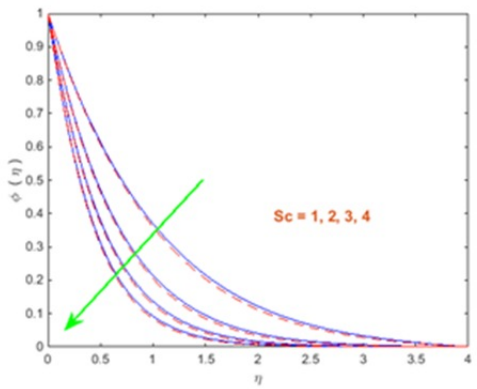

Figure 18: Profile $\phi(\eta)$ with the parameter Sc

Table 4: Change in Nusselt number with the parameters Pr, Bi, ϕ_1, ϕ_2 and ϕ_3.

		Parameters			N_{u_x}		
Pr	Bi	ϕ_1	ϕ_2	ϕ_3	Ag/Pfin	MoS_2/Pfin	Cu/Pfin
0.1					0.21210429	0.21253730	0.21153231
0.3					0.21534968	0.21651327	0.21151311
0.5					0.21849536	0.22034062	0.20034036
0.7					0.22154119	0.22401968	0.19411961

	0.1				0.11580783	0.11711188	0.10712131
	0.2				0.20395587	0.20816766	0.19816743
	0.3				0.27258401	0.28037702	0.25037721
	0.4				0.32715289	0.33870266	0.30870232
		0.01			0.22202707	0.28725894	0.25725822
		0.05			0.24329934	0.31618701	0.30618712
		0.07			0.25460610	0.33160581	0.31160514
		0.09			0.26644504	0.34774599	0.32774527
			0.01		0.35610814	0.28037702	0.24037771
			0.02		0.45994795	0.35885243	0.33885252
			0.03		0.59289764	0.45964172	0.41964132
			0.04		0.76876439	0.59383273	0.49383274
				0.01	0.45618812	0.35618810	0.25614310
				0.03	0.55992793	0.45022792	0.35043791
				0.05	0.69283765	0.59283760	0.49283762
				0.07	0.86873436	0.76813131	0.51813130

Table 5: Change in Sherwood number with the parameters.

Parameters				Sh_x	
N_t	N_b	γ_0	Sc	Ag/Pfin	MoS_2/Pfin
0.1				0.72117719	0.72439119
0.3				0.67645900	0.66619129
0.5				0.67242465	0.64172526
0.7				0.72687118	0.66396310
	0.2			0.72117719	0.72439119
	0.4			0.75456363	0.75897166
	0.6			0.76722107	0.77221271
	0.8			0.77308645	0.77891102
		0.0		0.35190974	0.35912370
		0.3		0.51796822	0.52308669
		0.6		0.65821399	0.66194814
		0.9		0.78029039	0.78306764
			1	0.94329594	0.95020807
			2	1.37244323	1.38554068
			3	1.70584087	1.72315856
			4	1.98672100	2.00735495

5. Conclusions

In this study, the thermal and flow behavior of nanofluids containing silver (Ag), copper (Cu), and molybdenum dioxide (MoS_2) nanoparticles suspended in paraffin as the base fluid has been analyzed under the influence of slip effects and convective boundary conditions. The governing model was solved numerically through the order reduction method, leading to several key insights. It is observed that all

nanoparticle types enhance the thermal performance, with MoS_2 exhibiting a particularly pronounced effect due to its higher volume fraction contribution. The velocity components were found to decrease with an increase in the rotation parameter, highlighting the damping influence of rotation. Moreover, temperature variations reveal that the magnetic parameter significantly impacts MoS_2 nanofluids, while Ag nanoparticles display comparatively moderate thermal responses. The thermophoretic parameter was shown to reduce shear stress, indicating its role in altering near-wall flow resistance. Additionally, the concentration profiles decline for larger Schmidt numbers and higher chemical reaction parameters, underlining the combined influence of mass diffusivity and reactive effects. Overall, these findings emphasize the importance of nanoparticle selection and parameter tuning in optimizing nanofluid systems for advanced thermal management applications.

References

1. Du, W., Luo, L., Wang, S., Liu, J., and Sunden, B., Heat transfer and flow structure in a rotating duct with detached pin fins, *Numerical Heat Transfer, Part A: Applications*, **75**(4), 217–241, (2019). https://doi.org/10.1080/10407782.2019.158095710.1080/10407782.2019.1580957.

2. Reddy, M. G., Dinesh, P. A., and Basavaraj, 3D rotating flow of Casson fluid over an elongated surface with thermophoresis and Brownian motion: Buongiorno Model, *Journal of Nanofluids*, **8**, 1479–1484, (2019).

3. Srilatha, P., Remidi, S., Nagapavani, M., Singh, H., and Prasannakumara, B. C., Heat and mass transfer analysis of a fluid flow across the conical gap of a cone-disk apparatus under thermophoretic particle motion, *Energies*, **16**, 952, (2023).

4. Turkyilmazoglu, M., The flow and heat transfer in the conical region of a rotating cone and an expanding disk, *International Journal of Numerical Methods for Heat & Fluid Flow*, (2023). https://doi.org/10.1108/HFF-11-2022-065510.1108/HFF-11-2022-0655.

5. Shahzad, F., Jamshed, W., Sajid, T., Nisar, K. S., and Mohamed Eid, R., Heat transfer analysis of MHD rotating flow of Fe_3O_4 nanoparticles through a stretchable surface, *Communications in Theoretical Physics*, **73**(7), 075004, (2021). https://doi.org/10.1088/1572-9494/abf8a110.1088/1572-9494/abf8a1.

6. Shah, Z., Islam, S., Gul, T., Bonyah, E., and Khan, M. A., Electrical MHD and Hall current impact on micropolar nanofluid flow between rotating parallel plates, *Results in Physics*, **9**, 1201–1214, (2018). https://doi.org/10.1016/j.rinp.2018.01.06410.1016/j.rinp.2018.01.064.

7. Hussain, A., Alshbool, M. H., Abdussattar, A., Rehman, A., Ahmad, H., Nofal, T. A., and Khan, M. R., A computational model for hybrid nanofluid flow on a rotating surface in the existence of convective condition, *Case Studies in Thermal Engineering*, **26**, 101089, (2021). https://doi.org/10.1016/j.csite.2021.10108910.1016/j.csite.2021.101089.

8. Mushtaq, A., and Mustafa, M., Computations for nanofluid flow near a stretchable rotating disk with axial magnetic field and convective conditions, *Results in Physics*, **7**, 3137–3144, (2017). https://doi.org/10.1016/j.rinp.2017.08.03110.1016/j.rinp.2017.08.031.

9. Das, S., Tarafdar, B., Jana, R. N., and Makinde, O. D., Magnetic ferro-nanofluid flow in a rotating channel containing Darcian porous medium considering induced magnetic field and Hall currents, *Special Topics & Reviews in Porous Media*, **10**(4), 357–383, (2019).

10. Moatimid, G. M., Mohamed, M. A. A., and Elagamy, K. A., Casson nanofluid flow within the conical gap between rotating surfaces of a cone and a horizontal disc, *Scientific Reports*, **12**, 11275, (2022). https://doi.org/10.1038/s41598-022-15094-w10.1038/s41598-022-15094-w.

11. Berrehal, H., and Maougal, A., Entropy generation analysis for multi-walled carbon nanotube (MWCNT) suspended nanofluid flow over a wedge with thermal radiation and convective boundary condition, *Journal of Mechanical Science and Technology*, **33**, 459–464, (2019). https://doi.org/10.1007/s12206-018-1245-y10.1007/s12206-018-1245-y.

12. Rejvani, M., Heidari, A., and Seadodin, S., Simultaneous effects of MWCNT and SiO_2 on the rheological behavior of cooling oil and sensitivity analysis, *Heliyon*, **9**(2), e12942, (2023). https://doi.org/10.1016/j.heliyon.2023.e1294210.1016/j.heliyon.2023.e12942.

13. Qureshi, M. Z. A., Faisal, M., Raza, Q., Ali, B., Botmart, T., and Shah, N. A., Morphological nanolayer impact on hybrid nanofluid flow due to dispersion of polymer/CNT matrix nanocomposite material, *AIMS Mathematics*, **8**(1), 633–656, (2023). https://doi.org/10.3934/math.202303010.3934/math.2023030.

14. Buffa, A., Erel, Y., and Mandler, D., Carbon nanotube-based flow-through electrochemical cell for electroanalysis, *Analytical Chemistry*, **88**(22), 11007–11015, (2016).

15. Seyedi, H. S., Saray, B. N., and Ramazani, A., High-accuracy multiscale simulation of three-dimensional squeezing carbon nanotube-based flow inside a rotating stretching channel, *Mathematical Problems in Engineering*, Article ID 9890626, (2019). https://doi.org/10.1155/2019/989062610.1155/2019/9890626.

16. Shashikumar, N. S., Gireesha, B. J., Mahanthesh, B., and Prasannakumara, B. C., Brinkman–Forchheimer flow of SWCNT and MWCNT magneto-nanoliquids in a microchannel with multiple slips and Joule heating aspects, *Multidiscipline Modeling in Materials and Structures*, **14**(4), 769–786, (2018). https://doi.org/10.1108/MMMS-01-2018-000510.1108/MMMS-01-2018-0005.

17. Gireesha, B. J., Prasannakumara, B. C., Umeshaiah, M., and Shashikumar, N. S., Three-dimensional boundary layer flow of MHD Maxwell nanofluid over a non-linearly stretching sheet with nonlinear thermal radiation, *Journal of Applied Nonlinear Dynamics*, **10**(2), 263–277, (2021). https://doi.org/10.5890/JAND.2021.06.00610.5890/JAND.2021.06.006.

18. Prasannakumara, B. C., Shashikumar, N. S., and Venkatesh, P., Boundary layer flow and heat transfer of nanofluid with fluid particle suspension over a nonlinear stretching sheet in the presence of thermal radiation, *Nonlinear Engineering*, **6**(3), 179–190, (2017). https://doi.org/10.1515/nleng-2017-000410.1515/nleng-2017-0004.

19. Madhu, M., Shashikumar, N. S., Thriveni, K., Gireesha, B. J., and Mahanthesh, B., Irreversibility analysis of the MHD Williamson fluid flow through a microchannel with thermal radiation, *Waves in Random and Complex Media*, (2022). https://doi.org/10.1080/17455030.2022.211147310.1080/17455030.2022.2111473.

20. Shashikumar, N. S., Thriveni, K., Madhu, M., Mahanthesh, B., Gireesha, B. J., and Kishan, N., Entropy generation analysis of radiative Williamson fluid flow in an inclined microchannel with multiple slip and convective heating boundary effects, *Proceedings of the Institution of Mechanical Engineers, Part E: Journal of Process Mechanical Engineering*, (2021). https://doi.org/10.1177/0954408921104986310.1177/09544089211049863.

21. Alktranee, M., Shehab, M. A., Németh, Z., Bencs, P., and Hernadi, K., Effect of zirconium oxide nanofluid on the behaviour of photovoltaic–thermal system: An experimental study, *Energy Reports*, **9**, 1265–1277, (2023). https://doi.org/10.1016/j.egyr.2022.12.06510.1016/j.egyr.2022.12.065.

22. Souayeh, B., Simultaneous features of C–C heat flux on dusty ternary nanofluid (Graphene + Tungsten Oxide + Zirconium Oxide) through a magnetic field with slippery condition, *Mathematics*, **11**, 554, (2023). https://doi.org/10.3390/math1103055410.3390/math11030554.

23. Cheng, H., Jianxun, S., Cheng, L., Lina, W., Changchun, Z., and Xingdong, Z., Synthesis of nano zirconium oxide and its application in dentistry, *Nanotechnology Reviews*, **8**(1), 396–404, (2019). https://doi.org/10.1515/ntrev-2019-003510.1515/ntrev-2019-0035.

24. Sun, C., Fard, B. E., Karimipour, A., Abdollahi, A., and Quang-Vu, B., Producing ZrO_2/LP107160 nanofluid and presenting a correlation for prediction of thermal conductivity via GMDH method: An empirical and numerical investigation, *Physica E: Low-Dimensional Systems and Nanostructures*, **127**, 114511, (2021). https://doi.org/10.1016/j.physe.2020.11451110.1016/j.physe.2020.114511.

25. Guzei, D. V., Minakov, A. V., and Popov, I. A., Experimental and numerical study of nanofluid forced convection in a channel with artificial roughness, *Journal of Physics: Conference Series*, **1105**, 012133, (2018).

26. Tiwari, R. K., and Das, M. K., Heat transfer augmentation in two-sided lid-driven differentially heated square cavity utilizing nanofluids, *International Journal of Heat and Mass Transfer*, **50**, 2002–2018, (2007).

27. Oztop, H. F., and Abu-Nada, E., Numerical study of natural convection in partially heated rectangular enclosures with nanofluids, *International Journal of Heat and Fluid Flow*, **29**, 1326–1336, (2008).

28. Ahmad, S., Younis, J., Ali, K., Rizwan, M., Ashraf, M., Abd El Salam, M. A., Impact of swimming gyrotactic microorganisms and viscous dissipation on nanoparticles flow through a permeable medium – A numerical assessment, *Journal of Nanomaterials*, 4888128, (2022). https://doi.org/10.1155/2022/488812810.1155/2022/4888128.

29. Ahmad, S., Akhter, S., Shahid, M. I., Ali, K., Akhtar, M., Ashraf, M., Novel thermal aspects of hybrid nanofluid flow comprising manganese zinc ferrite ($MnZnFe_2O_4$), nickel zinc ferrite ($NiZnFe_2O_4$) and motile microorganisms, *Ain Shams Engineering Journal*, **13**(5), 101668, (2022). https://doi.org/10.1016/j.asej.2021.10166810.1016/j.asej.2021.101668.

30. Ahmad, S., Ali, K., Rizwan, M., and Ashraf, M., Heat and mass transfer attributes of copper–aluminum oxide hybrid nanoparticles flow through a porous medium, *Case Studies in Thermal Engineering*, **25**, 100932, (2021). https://doi.org/10.1016/j.csite.2021.10093210.1016/j.csite.2021.100932.

31. Ahmad, S., Ali, K., Ashraf, M., Abd El-Wahed Khalifa, H., ElSeabee, F. A. A., and El Sayed, M. Din, Analysis of pure nanofluid (GO/engine oil) and hybrid nanofluid (GO–Fe_3O_4/engine oil): Novel thermal and magnetic features,*Nanotechnology Reviews*, **11**, 2903–2915, (2022).

32. Acharya, N., Das, K., and Kundu, P. K., Rotating flow of carbon nanotube over a stretching surface in the presence of magnetic field: A comparative study, *Applied Nanoscience*, **8**, 369–378, (2018). https://doi.org/10.1007/s13204-018-0794-910.1007/s13204-018-0794-9.

33. Ali, H., Shabir, G., Ahmad, Z., Qayyum, Y., and Qayyum, A., Mixed Convection in a Casson Fluid Flow towards a Heated Shrinking Surface, *Earthline Journal of Mathematical Sciences*, **13**(2), 413–429, (2023). https://doi.org/10.34198/ejms.13223.413429.

Sakeena Bibi,

Department of Mathematics,

Faculty of Sciences, The University of Faisalabad, Faisalabad,

Pakistan.

E-mail address: sakinaaziz2019@gmail.com

and

Mukhtar Ahmad,
Department of Computer Science and Mathematics,
Universiti Malaysia Terengganu 21030 Kuala Nerus, Terengganu,
Malaysia.
E-mail address: itxmemuktar@gmail.com

and

Muhammad Muawwaz,
Department of Mathematics,
Riphah International University, Faisalabad Campus, Faisalabad,
Pakistan.
E-mail address: muawwaz123@gmail.com

and

Fouzia Sadaf,
Department of Mathematics,
University of Southern Punjab, Multan,
Pakistan.
E-mail address: fouziasadaf46@gmail.com

and

Ather Qayyum,
Institute of Mathematical Sciences,
Faculty of Science, Universiti Malaya,
Malaysia
and
Mechanical Engineering Department,
College of Engineering, Gulf University,
Sanad 26489 Kingdom of Bahrain.
E-mail address: dratherqayyum@um.edu.my